Chinese Chemical Letters 35 (2024) 109223

Contents lists available at ScienceDirect

Chinese Chemical Letters

journal homepage: www.elsevier.com/locate/cclet

HSA shrinkage optimizes the photostability of embedded dyes fundamentally to amplify their efficiency as photothermal materials

Yongkang Yue[a], Zhou Xu[a,b], Kaiqing Ma[a], Fangjun Huo[c], Xuemei Qin[b], Kuanshou Zhang[d], Caixia Yin[a,*]

[a] Department Key Laboratory of Chemical Biology and Molecular Engineering of Ministry of Education, Institute of Molecular Science, Shanxi University, Taiyuan 030006, China
[b] Department Modern Research Center for Traditional Chinese Medicine, Shanxi University, Taiyuan 030006, China
[c] Research Institute of Applied Chemistry, Shanxi University, Taiyuan 030006, China
[d] State Key Laboratory of Quantum Optics and Quantum Optics Devices, Institute of Opto-Electronics, Shanxi University, Taiyuan 030006, China

ARTICLE INFO

Article history:
Received 11 August 2023
Revised 15 October 2023
Accepted 19 October 2023
Available online 20 October 2023

Keywords:
Photothermal therapy
Cyanine dyes
Photostability
Albumin
Encapsulation

ABSTRACT

Focused on the performance promotion of organic small molecular dyes based photothermal agents *via* non-chemical modification, we found that heat-assisted binding of human serum albumin (HSA) to the dye causes shrinkage of the protein and encapsulate the dye to form nanoparticles. This revolutionizes the photostability of small molecule dyes which further improves their photothermal conversion efficiency and tumor ablation performance as photothermal agents significantly. In this work, the obtained photothermal agent named HSA-P2-T could accumulate in tumor and induce 22 °C enhancement of the tumor in xenograft models upon ultra-low dose (0.1 W/cm^2) laser irradiation, which, as far as we know, is the lowest laser dose used *in vivo* photothermal therapy. Utilizing HSA-P2-T, we realized tumor ablation upon twice intravenous injections of the nanoparticles and four photothermal treatments.

Photothermal therapy (PTT) relies on the photothermal effect of photothermal agents to convert light into heat which further triggers the death of cancer cells *via* a relatively noninvasive manner [1–3]. As a key component of the therapy, photothermal agents confined the actual therapeutic effect by their photophysical properties and photochemical stabilities [4,5]. Typically, an ideal photothermal agent for efficient PTT should hold the features such as high molar extinction coefficient to support sufficient photothermal performance, moderate blood retention time and high cancer accumulation rate to promote cancer ablation precisely, and high photostability and minimized biological toxicity to support multiple irradiations while avoid the damage to healthy tissues, *etc.* [1,6–9]. Up to now, the major members of photothermal agents are inorganic materials such as noble metal materials and carbon-based nanomaterials due to their excellent photostability and photothermal conversion efficiency [10–12]. However, their chemical inertness in turns caused nonbiodegradable of these materials which further resulted in a long-term toxicity risk [13,14].

Comparing with these inorganic materials, organic small molecular dyes hold great potential to construct biodegradable photothermal agents promoted by their easily modified nature, tunable absorption, and accessible structure–property relationships [6,15–18]. However, for most of the organic small molecular dyes, the photo-functional applications are seriously affected by their photobleaching properties which are more significance for fluorescent dyes in near infrared band [6,19,20]. For PTT, the photobleaching of dyes not only attenuated the photothermal efficiency through dyes degradation during laser irradiation, but also restricted multiple PTT upon once injection. In that case, repeated administration of photothermal agents would increase their accumulation in healthy organs with amplified toxicity [21]. Thus, improving the photostability of organic small molecular dyes might be a breakthrough to fit the actual applications.

Actually, photobleaching generally results from the irreversible destruction of the fluorophore by surrounding molecules, especially oxygen, when the fluorophore is in the excited state [22]. Thus, we anticipated that protein encapsulation of organic small molecular dyes might block the surrounding oxygen in solution and improve their photostability. Human serum albumin (HSA) features multiple molecular binding sites for both endogenic and exogenous species [23,24]. Upon HSA modification, the dispersion and biocompatibility of most exogenous organic compounds were improved effectively [25–27]. Besides, HSA modification formed

* Corresponding author.
E-mail address: yincx@sxu.edu.cn (C. Yin).

https://doi.org/10.1016/j.cclet.2023.109223
1001-8417/

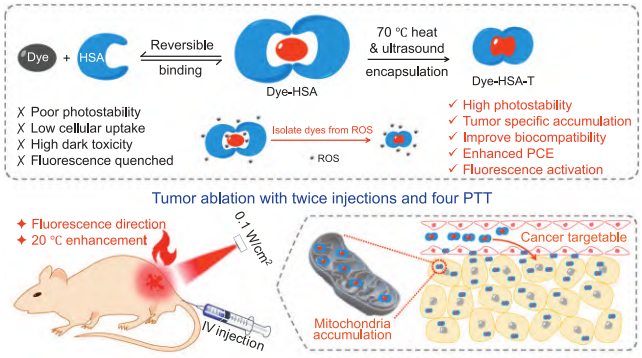

Fig. 1. Non-chemical modification method to restrain the photobleaching of organic small molecular dyes and improve their performance as photothermal agents.

nano particles could deliver exogenous compounds to tumor *via* the synergy of enhanced permeability and retention (EPR) of tumor tissue and the expression of the albumin-binding proteins including the gp60 receptor and secreted protein, acidic and rich in cysteine (SPARC) in tumor tissue [28,29]. These peculiarities promoted HSA as preferred cage for the development of efficient photothermal agents based on organic small molecular dyes.

In this work, we synthesized four cyanine dyes. All of these dyes displayed significant photothermal effect under 660 nm laser irradiation. However, these dyes were bleached after the first irradiation–cooling cycle. Their photobleaching fate could be reversed upon encapsulation in HSA. Typically, instead of the previously used spontaneous binding of dyes and HSA under physiological condition, heating of the bound complex would shrink the protein and encapsulate the dyes tightly to avoid their photobleaching completely (Fig. 1). We selected P2, a cell membranes permeable dye with lowest cytotoxicity, as the preferred dye to obtain the spherical nanoparticles named HSA-P2-T with a particle size of about 3 nm. The corresponding photothermal conversion efficiency (PCE) was calculated to be 64.5%, which is higher than most of the organic small molecular dyes based photothermal agents [10,30]. Moreover, HSA-P2-T enriched in mitochondria, which is regarded as the most sensitive organelle toward hyperthermia, to induce cell death upon laser irradiation [7,31,32]. In the following *in vivo* imaging and therapeutic experiments, we found that HSA-P2-T could accumulate in tumor efficiently after intravenous (IV) injection and ablate it upon twice injections and four ultra-low dose (0.1 W/cm^2) laser irradiation.

Compared with rhodamine and other fluorescent dyes, cyanine dyes feature high molar extinction coefficient and low fluorescence quantum yield, which make them widely concerned in the preparation of photothermal conversion materials and photoacoustic imaging materials. However, similar to many small molecular fluorescent dyes, the polyolefin structure of cyanine is especially vulnerable to oxidation and bleaching by reactive oxygen species. In this work, we synthesized four asymmetric cyanine-3 (Cy-3) derivatives. All of these asymmetric Cy-3 dyes displayed significant photothermal effect in phosphate buffered saline (PBS) upon laser irradiation. To evaluate their potential as photothermal reagents for tumor PTT, we evaluated the dark- and photo-toxicity of these compounds in HCT-116 cells, respectively. We found that, similar to most of the small molecule organic dyes containing carboxyl groups, carboxyl modified compounds P1 and P3 showed little dark- and photo-toxicity due to their poor cell membrane permeability. The quandary was efficiently improved in the esterification products named P2 and P4. As shown in Fig. 2, incubation of cells with 10 μmol/L P2 for 30 min resulted in 50% cell death after 5 min of laser irradiation at 660 nm. The phototoxicity of P2 toward HCT-116 cells aggravated along with the increasing dye concentrations. At the same time, its biocompatibility without laser irradiation could be highlighted by the negligible decrease in cell viability after being treated with 40 μmol/L P2 for 12 h. For the thiazolium substituted Cy-3 derivative P4, however, both of its dark- and photo-toxicity are significant. P2 and P4 displayed similar dark and photo-toxicity results of on the murine 4T1 cells (Fig. S1 in Supporting information). Therefore, P2 was selected as the photothermal agent in the following photothermal experiments.

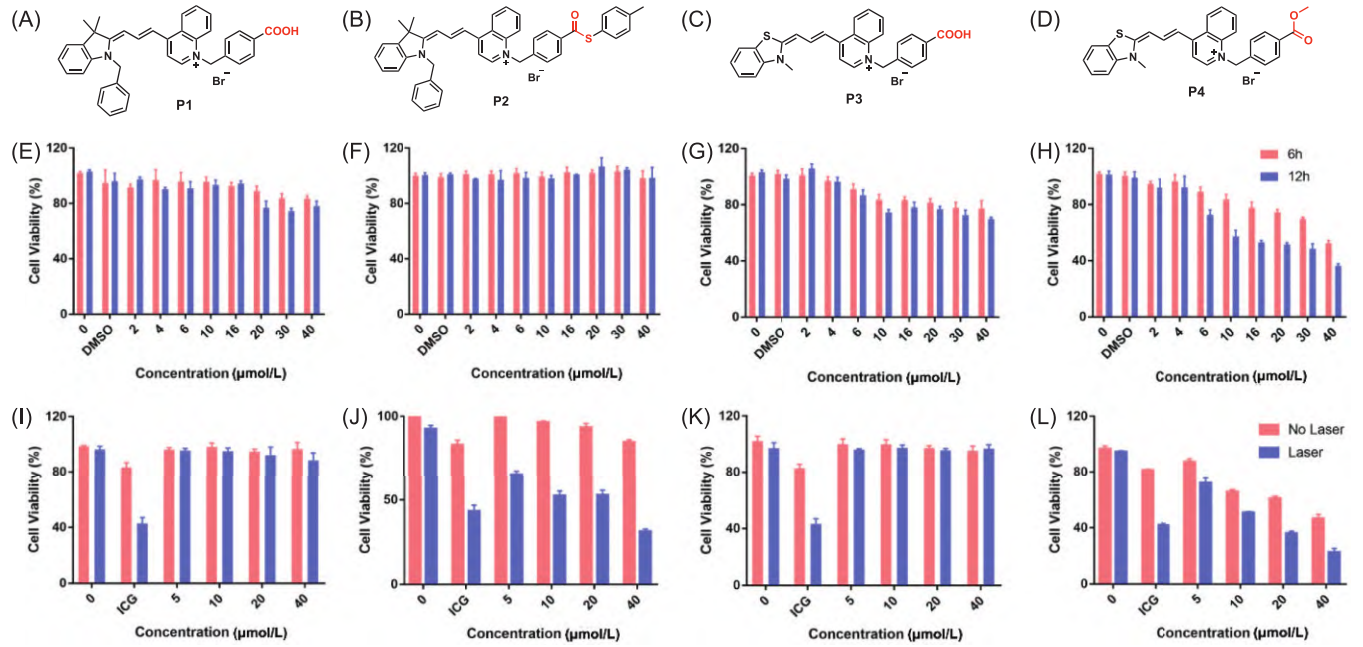

Fig. 2. (A–D) The chemical structures of the asymmetric Cy-3 dyes synthesized in this work. (E–H) The corresponding cytotoxicity of the four dyes upon 6 h and 12 h incubation, respectively. (I–L) The dark- and photo-toxicity comparation of the four dyes upon 30 min incubation followed by 5 min laser irradiation. ICG with 40 μmol/L was used as control compound in (I-L). 660 nm laser with 0.45 W/cm^2 power density was used in these experiments. Error bars represent standard deviations obtained from three independent experiments.

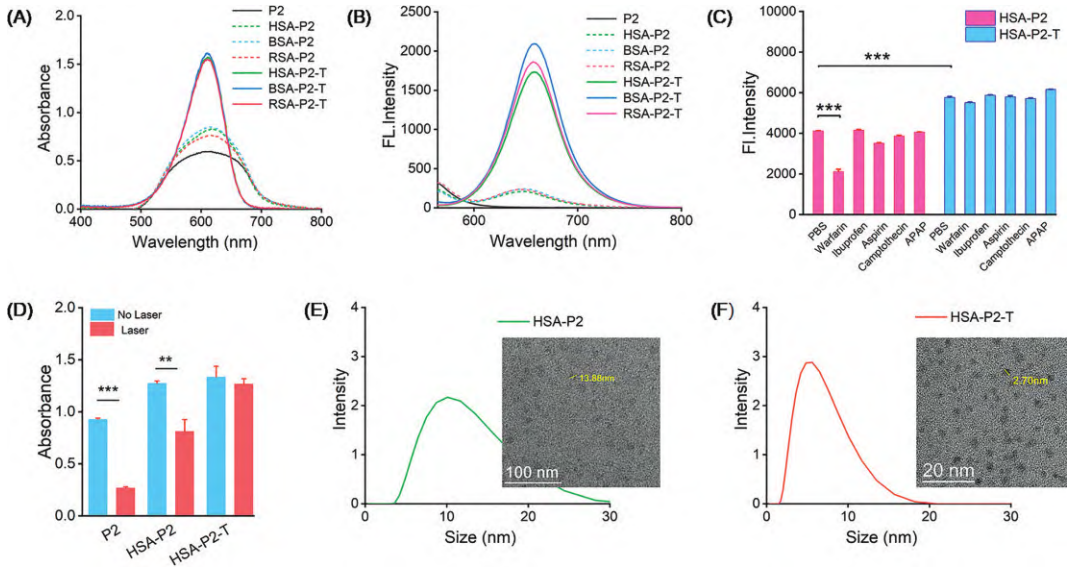

Fig. 3. HSA modification to improve the photostability of P2. (A) Ultraviolet-visible and (B) fluorescence responses of P2 (40 μmol/L) toward HSA, BSA and RSA in PBS. (C) Fluorescence intensity changes of HSA-P2 and HSA-P2-T system at 650 nm upon addition of 400 μmol/L competitive compounds including ibuprofen, warfarin, acetaminophen (APAP), aspirin, and camptothecin, respectively. (D) Absorbance (600 nm) changes of 40 μmol/L P2, HSA-P2 and HSA-P2-T in PBS with or without 5 min laser irradiation (660 nm, 0.2 W/cm^2). Dynamic light scattering data and transmission electron microscopy images of HSA-P2 (E) and HSA-P2-T (F). $\lambda_{ex} = 600$ nm. Error bars represent standard deviations obtained from three independent experiments. Statistical analyses were performed with Student's *t*-test, $^{**}P < 0.01$, $^{***}P < 0.001$.

We then evaluated the laser power density and irradiation time dependent cell viability changes of HCT-116 cells after 30 min incubation of 40 μmol/L P2. Upon 5 min of laser irradiation, the cell mortality rate was positively correlated with the laser power density (Fig. S2A in Supporting information). Considering the negligible phototoxicity of the utilized laser (Fig. 2), we selected 0.45 W/cm^2 as a standard laser power density in the *in vitro* experiments. In the following irradiation time dependency evaluation, we found that the cell viability decreased in the first 5 min irradiation range (Fig. S2B in Supporting information). However, extension of the irradiation time did not induce further cell death under the same conditions. Actually, the absorption band of P2 in PBS was significantly reduced under similar irradiation condition which meant the photobleaching of the dye. Thus, to improve the photostability of P2 might support a long-term laser irradiation and amplify its performance in PTT.

HSA as the most abundant protein in serum has widely been used as vehicles to delivery drugs or contrast agents for diseases diagnosis and treatment, such as the clinical used albumin bound Paclitaxel. We anticipated that HSA might bind P2 spontaneously to protect the dye in solution and improve its photostability. So, we added HSA in P2 containing PBS solution and monitored the optical changes. As shown in Fig. 3A, P2 displayed a broad absorption band centered at 600 nm. After HSA addition, the absorbance at 600 nm increased distinctively, and the corresponding full width at half maxima (FWHM) decreased. Along with the absorbance changes, HSA addition induced turn on fluorescence signal of P2 at 650 nm in PBS (Fig. 3B). Bovine serum albumin (BSA) and rat serum albumin (RSA) could also bind P2 with similar optical responses. These results confirmed that albumin could bind P2 in aqueous solution spontaneously. So, we further evaluated the binding molar ratio and binding site of albumin to P2. The fluorescence intensity changes at 650 nm were elected to indicate the binding of HSA and P2. HSA bound P2 with a molar ratio of 2:1 based on the equimolar method (Fig. S3B in Supporting information). The corresponding binding site was analyzed by the competitive inhibition experiments upon addition of the reported HSA non-covalent binding compounds with different binding domains to HSA-P2 system [33]. We noticed that warfarin, a typical anticoagulant that binds to the drug site I of HSA with high affinity, could inhabit the fluorescence enhancement efficiently (Fig. 3C) [34,35]. At the same time, aspirin (drug site I) with lower binding constant could also inhabit the spontaneous binding of HSA and P2 to some extent [36,37]. Fig. S4 (Supporting information) displayed the corresponding energetic favorable molecular docking result. Other compounds such as ibuprofen, camptothecin and paracetamol did not inhabit the binding process. Thus, P2 was proposed to bind to drug site I of HSA. These results also suggested that the non-covalent bound dye could escape from the subdomain of HSA dynamically to reduce the protective effect. To further strengthen their binding and encapsulate P2 in HSA, we heated the HSA-P2 solution at 70 °C for 10 min to constringe the protein while preserving its water solubility and dispersibility [26]. Indeed, there was no tendency for the heated HSA-P2 system (HSA-P2-T) to be inhibited by the competing drugs (Fig. 3C). The heat process brought 58% K_a enhancement comparing HSA-P2-T with HSA-P2 (Fig. S5 in Supporting information). With similar optical properties to HSA-P2, HSA-P2-T features higher absorbance at 600 nm and lower FWHM (Fig. 3A). This means the gradual transition from the aggregate state to the monomer of P2. Transmission electron microscopy analysis showed that both HSA-P2 and HSA-P2-T were spherical in shape, but with different diameters which were further verified by the dynamic light scattering tests (Figs. 3E and F, approximately 14 nm for HSA-P2 and 3 nm for HSA-P2-T, respectively). We utilized the absorbance changes of P2, HSA-P2 and HSA-P2-T at 600 nm to evaluate their photostability upon laser irradiation. As shown in Fig. 3D, 5 min laser irradiation induced 70% P2 and 40% HSA-P2 quenching in PBS. However, the photobleaching fate of the dye was reversed in the HSA-P2-T case and only 3% HSA-P2-T was quenched under same irradiation condition. These results confirmed that comparing with the traditional spontaneous binding of dyes with HSA, 70 °C heating reinforced the spontaneous binding and brought significant photostability improvement *via* a non-chemical modification way.

The feasibility of HSA encapsulation to improve the photostability of P2 and amplify its performance in PTT was then verified upon laser irradiation of P2, HSA-P2 and HSA-P2-T in PBS, respectively. As shown in Figs. S6A–C (Supporting information), the

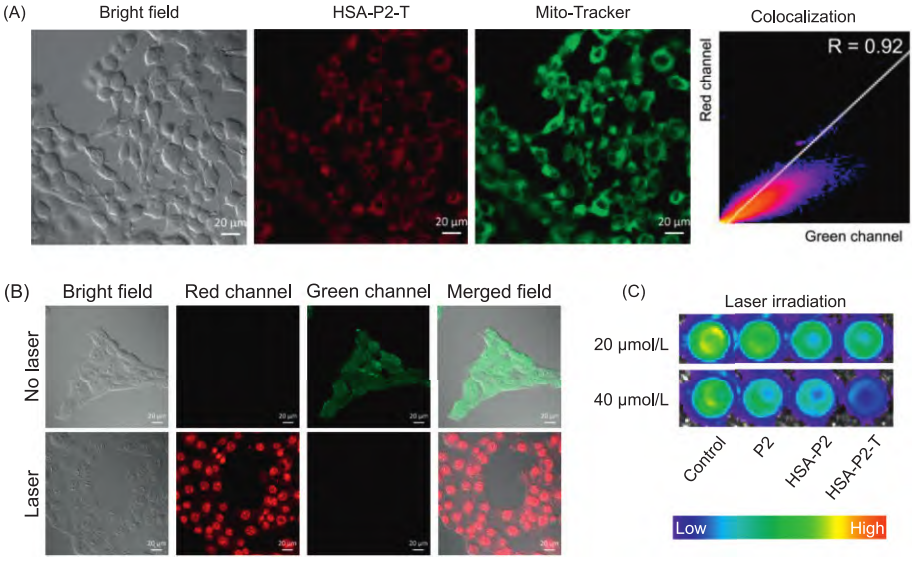

Fig. 4. Cell imaging experiments to evaluate the distribution of HSA-P2-T in cells and the photothermal effect induced cell death. (A) Dual-channel fluorescence imaging of 4T1 cells co-stained of with HSA-P2-T and Mito-Tracker green (1 μmol/L). The Pearson's coefficient was obtained by ImageJ based on the fluorescence images. Green channel: $\lambda_{em} = 510–536$ nm; Red channel: $\lambda_{em} = 606–666$ nm. (B) Dual-channel fluorescence imaging of HSA-P2-T pre-incubated 4T1 cells after co-stained with Calcein-AM and PI. Green channel: $\lambda_{em} = 420–520$ nm; Red channel: $\lambda_{em} = 540–600$ nm. (C) Laser irradiation induced cell viability changes of HSA-P2-T loaded HCT-116 cells by a chemiluminescence cell viability assay kit. The concentrations of P2 and HSA were 10 and 20 μmol/L, respectively.

first 5 min irradiation resulted similar temperature enhancement of the three solutions. However, similar to the aforementioned absorbance changes, P2 and HSA-P2 showed a 45% and 10% attenuation in temperature response in the third irradiation-cooling cycles, respectively. For HSA-P2-T, no change was detected in the temperature plateau after three irradiation–cooling cycles, confirming the anticipation to improve the photothermal performance of P2 upon HSA encapsulation. Besides, the HSA engineering to improve anti-photobleaching property and photothermal performance of organic dyes could also be seen in the P1 bound system (Fig. S7 in Supporting information). Interestingly, along with the photostability improvement, the cell uptake rate and cell compatibility of HSA-P2-T were also significantly improved (Figs. S6D–F in Supporting information). Besides, the PCE of P2, HSA-P2 and HSA-P2-T were calculated to be 45.4%, 46.5% and 64.5%, respectively (Fig. S8 in Supporting information) [30]. Thus, HSA-P2-T holds great potential to be utilized as high performance photothermal reagent based on small molecule dye.

Since cyanine dyes are well used mitochondria targetable fluorescence dyes, we wondered that HSA encapsulation might retain the mitochondria targeting potential of the dye and accumulate in mitochondria [38–40], which is reported as the most sensitive organelle toward hyperthermia, to proceed efficient PTT [41]. HSA-P2-T entered cells efficiently and lightened cells with distinct fluorescence signal in the red channel (606–666 nm). At the same time, the fluorescence signal of HSA-P2-T overlapped with that of the Mito-Tracker green with a Pearson's *R* of 0.92 (Fig. 4A). The potential of HSA-P2-T as efficient photothermal agent for PTT was also evaluated by fluorescence imaging-based cell viability kit. As shown in Fig. 4B, laser free HSA-P2-T loaded 4T1 cells displayed significant fluorescence signal in the green channel while undetectable signal in the red channel after co-staining with calcein-AM (stains live cells with green fluorescence signal) and propidium iodide (PI, stains nucleus of dead cells with red fluorescence signal) [42]. However, after laser irradiation, only the nucleus of 4T1 cells displayed fluorescence signal. To further confirm that the fluorescence nature of HSA-P2-T did not interfere the former fluorescence imaging results, we utilized a chemiluminescence cell viability assay kit to evaluate the cell viability after dyes incubation. Upon same concentration of dyes incubation and laser irradiation, the chemiluminescence signals of HCT-116 cells reflected the largest decrease in cell viability induced by HSA-P2-T (Fig. 4C). Supported by the *in vitro* results, we evaluated the tumor targetable property of HSA-P2-T proposed by the synergetic EPR effect of nano particles and active uptake through albumin-binding proteins. As shown in Fig. S9 (Supporting information), the fluorescence signal of the tumor enhanced significantly within 2.5 h after IV injection of HSA-P2-T and retained in the following 20 h. The *ex vivo* organs fluorescence imaging also supported the tumor accumulation of HSA-P2-T after IV injection (Fig. S10 in Supporting information). Thus, HSA-P2-T features several key properties such as minimal dark cytotoxicity, mitochondria targetable, ultrahigh photostability, high phototoxicity and tumor targetable to be utilized as favorable photothermal agent for PTT.

To evaluate the PTT based therapeutic effect of HSA-P2-T *in vivo*, we constructed xenograft tumor models by subcutaneous injection of 4T1 cells and administrated PBS, P2 and HSA-P2-T *via* IV injection, respectively. In a preliminary experiment, we used a 660 nm laser with 0.2 W/cm^2 (the lowest laser power density utilized for organic small molecular dyes centered photothermal agents, as far as we know) light intensity to irradiate the tumor regions [6,7,30,43–45]. As shown in Fig. S11B (Supporting information), mice injected with PBS displayed minor temperature enhancement (about 3 °C) in the tumor region upon laser irradiation. The temperature changes might be induced by the self-absorption of the tissue and blood at 660 nm [46,47]. However, surprisingly, the HSA-P2-T injection group resulted about 40 °C enhancement over the tumor region within 5 min irradiation (Figs. S11B and C in Supporting information). So, to ensure the laboratory animal welfare, we further lowered the irradiation intensity (0.1 W/cm^2) in the following *in vivo* experiments. Fig. 5A illustrated the general procedures of these experiments. Upon 5 min irradiation, the tumor regions of P2 and HSA-P2-T injection group featured 10 and 22 °C enhancement, respectively (Fig. 5B). In contrast to the continuous tumor growth in PBS treatment group, the tumor growth was significantly inhibited in the P2 or HSA-P2-T injection group during the PTT course (Fig. 5C and Fig. S12 in Supporting information). Actually, the tumors in the HSA-P2-T

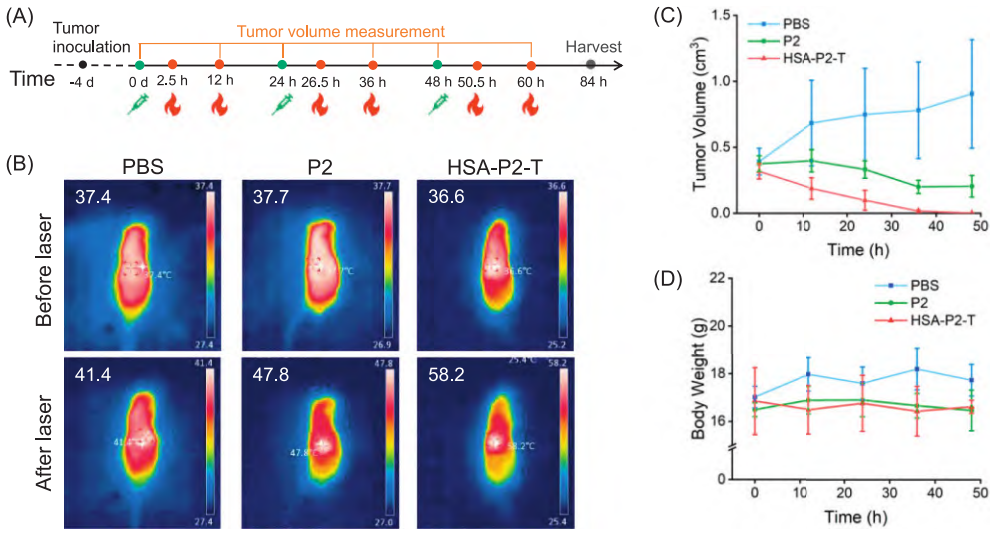

Fig. 5. *In vivo* PTT evaluation of HSA-P2-T in xenograft mice models. (A) Illustration of the procedures performed in these experiments. (B) Photothermal imaging of mice irradiated with 0.1 W/cm^2 laser for 5 min. The PTT were performed 2.5 and 12 h after IV injection of 100 μL PBS, P2 and HSA-P2-T, respectively. (C) Tumor volume changes of the three mice groups within the PTT. (D) Changes in body weight of each group of mice during PTT. The concentrations of P2 and HSA were 100 and 200 μmol/L, respectively. Error bars represent standard deviations obtained from three independent experiments.

injection group could be ablated entirely upon twice injections and four PTT. The corresponding tumors in the three group were harvested at the terminal of the experiments and we did not find any tumor tissue in the HSA-P2-T injection group (Fig. S13 in Supporting information).

Besides, during the PTT course, the body weight of the mice in each group remained stable, which meant that the dyes and light dose used were within the safe range for normal tissues of the mice (Fig. 5D). In addition, the biosafety of HSA-P2-T was also confirmed by hematoxylin-eosin staining of major organs of experimental mice (Fig. S14 in Supporting information). Thus, with excellent PTT performance, HSA-P2-T holds great potential to be utilized as biocompatible tumor specific ablation regent.

In this work, we synthesized four asymmetric Cy-3 dyes and evaluated their potential to be used as photothermal agents. We found that like most of the organic small molecular dyes, these Cy-3 dyes were easily photobleached upon laser irradiation. Their photobleaching fate could be reversed completely upon encapsulation in HSA. Actually, along with the photostability improvement, HSA encapsulation also endowed several qualities including improved PCE and cancer cell uptake rate, lowered dark cytotoxicity and activated fluorescence property that are key parameters to guarantee the prospect of efficient PTT of the dyes. The photothermal agent proposed in this work, HSA-P2-T, presented an 64.5% PCE and could accumulate in the mitochondria of cancer cells to perform PTT. In the *in vivo* PTT experiments, an ultra-low laser irradiation dose could induce about 22 °C enhancement over the tumor region within 5 min irradiation. Utilizing the HSA-P2-T, we realized the tumor ablation upon twice photothermal agent injection and four PTT. The present protocol makes up for the defect of poor photostability of organic small molecular dyes to be utilized as photo-functional materials, which has positive significance in promoting the therapeutic applications of these dyes.

Ethical statement

This study was performed in strict accordance with the Chinese guidelines for the care and use of laboratory animals and was approved by the Institutional Animal Care and Use Committee of Scientific Research in Shanxi University (No. SXULL2019033). HSA was purchased from Psaitong (ART No. H10013–1g).

Declaration of competing interest

The authors declare that they have no known competing financial interests or personal relationships that could have appeared to influence the work reported in this paper.

Acknowledgments

We thank the National Natural Science Foundation of China (Nos. 22277069, 22074084), Program of the State Key Laboratory of Quantum Optics and Optical Quantum Devices of Shanxi University (No. KF202108).

Supplementary materials

Supplementary material associated with this article can be found, in the online version, at doi:10.1016/j.cclet.2023.109223.

References

[1] Y. Liu, P. Bhattarai, Z. Dai, X. Chen, Chem. Soc. Rev. 48 (2019) 2053–2108.
[2] Z. Xie, T. Fan, J. An, et al., Chem. Soc. Rev. 49 (2020) 8065–8087.
[3] M. Ferrari, Nat. Rev. Cancer 5 (2005) 161–171.
[4] H. Si, D. Wang, X. Du, X. Zhou, Chin. Chem. Lett. 35 (2024) 108595.
[5] L. Wang, A. Mei, N. Li, et al., Chin. Chem. Lett. 35 (2024) 108974.
[6] H.S. Jung, P. Verwilst, A. Sharma, et al., Chem. Soc. Rev. 47 (2018) 2280–2297.
[7] J. Liu, J. Shi, W. Nie, et al., Adv. Healthc. Mater. 10 (2021) 2001207.
[8] K.X. Teng, W.K. Chen, L.Y. Niu, et al., Angew. Chem. Int. Ed. 60 (2021) 19912–19920.
[9] G. Feng, G.Q. Zhang, D. Ding, Chem. Soc. Rev. 49 (2020) 8179–8234.
[10] C. Xu, K. Pu, Chem. Soc. Rev. 50 (2021) 1111–1137.
[11] L.R. Hirsch, R.J. Stafford, J.A. Bankson, et al., Proc. Natl. Acad. Sci. U. S. A. 100 (2003) 13549–13554.
[12] D.P. O'Neal, L.R. Hirsch, N.J. Halas, J.D. Payne, J.L. West, Cancer Lett. 209 (2004) 171–176.
[13] B. Zhou, Y. Li, G. Niu, et al., ACS Appl. Mater. Interfaces 8 (2016) 29899–29905.
[14] L. Zou, H. Wang, B. He, et al., Theranostics 6 (2016) 762–772.
[15] M. Xing, Y. Han, Y. Zhu, et al., Anal. Chem. 94 (2022) 12836–12844.
[16] G. Yang, P. Li, Y. Han, et al., Mater. Chem. Phys. 295 (2023) 127145.
[17] L. Tang, P. Li, Y. Han, et al., J. Photochem. Photobiol. A: Chem. 438 (2023) 114511.
[18] H. Xin, Y. Huang, Y. Han, et al., Spectrochim. Acta Part A: Mol. Biomol. Spectrosc. 299 (2023) 122876.
[19] J.H.M. Van Der Velde, J. Oelerich, J. Huang, et al., Nat. Commun. 7 (2016) 10144.
[20] Z. Lei, F. Zhang, Angew. Chem. Int. Ed. 60 (2021) 16294–16308.
[21] P. Cheng, K. Pu, Nat. Rev. Mater. 6 (2021) 1095–1113.
[22] A.N. Butkevich, M.L. Bossi, G. Lukinavičius, S.W. Hell, J. Am. Chem. Soc. 141 (2019) 981–989.

[23] Y. Yue, T. Zhao, Y. Wang, et al., Chem. Sci. 13 (2022) 218–224.
[24] Y. Fan, F. Wang, F. Hou, et al., Chin. Chem. Lett. 34 (2023) 107557.
[25] S. Gao, G. Wei, S. Zhang, et al., Nat. Commun. 10 (2019) 2206.
[26] R. Tian, Q. Zeng, S. Zhu, et al., Sci. Adv. 5 (2019) eaaw0672.
[27] Y. Yue, T. Zhao, Z. Xu, et al., Adv. Sci. 10 (2023) 2205080.
[28] Q. Chen, Z. Liu, Adv. Mater. 28 (2016) 10557–10566.
[29] Z. Liu, X. Chen, Chem. Soc. Rev. 45 (2016) 1432–1456.
[30] H. Gu, W. Liu, W. Sun, et al., Chem. Sci. 13 (2022) 9719–9726.
[31] J. Zielonka, J. Joseph, A. Sikora, et al., Chem. Rev. 117 (2017) 10043–10120.
[32] J. Kadkhoda, A. Tarighatnia, N.D. Nader, A. Aghanejad, Life Sci. 307 (2022) 120898.
[33] Z. Luo, T. Lv, K. Zhu, et al., Angew. Chem. Int. Ed. 59 (2020) 3131–3136.
[34] I. Petitpas, A.A. Bhattacharya, S. Twine, M. East, S. Curry, J. Biol. Chem. 276 (2001) 22804–22809.
[35] G. Rabbani, S.N. Ahn, Int. J. Biol. Macromol. 123 (2019) 979–990.
[36] F. Yang, C. Bian, L. Zhu, et al., J. Struct. Biol. 157 (2007) 348–355.
[37] H. Alsamamra, K. Kh, S. Darwish, M. Abuteir, J. Med. Physiol. Biophys. 49 (2018) 1–8.
[38] K. Qian, H. Chen, C. Qu, et al., Nanomed. Nanotechnol. Biol. Med. 23 (2020) 102087.
[39] G. Battogtokh, Y.T. Ko, Nanomed. Nanotechnol. Biol. Med. 13 (2017) 733–743.
[40] S. Li, G. Zhang, Y. Peng, et al., Adv. Healthc. Mater. 12 (2023) 2300327.
[41] W. Sun, S. Guo, C. Hu, J. Fan, X. Peng, Chem. Rev. 116 (2016) 7768–7817.
[42] D. Xi, N. Xu, X. Xia, et al., Adv. Mater. 34 (2022) 2106797.
[43] W. Bian, Y. Wang, Z. Pan, et al., ACS Appl. Nano Mater. 4 (2021) 11353–11385.
[44] D. Xi, M. Xiao, J. Cao, et al., Adv. Mater. 32 (2020) 1907855.
[45] H. Dai, Z. Cheng, T. Zhang, et al., Chin. Chem. Lett. 33 (2022) 2501–2506.
[46] A.M. Smith, M.C. Mancini, S. Nie, Nat. Nanotechnol. 4 (2009) 710–711.
[47] J. Cao, B. Zhu, K. Zheng, et al., Front. Bioeng. Biotechnol. 7 (2020) 487.